Statistical Decomposition and Machine Learning to Clean In-Situ Spaceflight Magnetic Field Measurements

Matthew G. Finley[1], Trevor A Bowen[2], Marc Pulupa[3], Andriy Koval[4], and David Michael Miles[1]

[1]University of Iowa
[2]Space Sciences Laboratory
[3]Space Sciences Laboratory, University of California at Berkeley
[4]Goddard Planetary Heliophysics Institute, University of Maryland Baltimore County

March 16, 2023

Abstract

Robust in-situ magnetic field measurements are critical to understanding the various mechanisms that couple mass, momentum, and energy throughout our solar system. However, the spacecraft on which magnetometers are often deployed contaminate the magnetic field measurements via onboard subsystems including reaction wheels and magnetorquers. Two magnetometers can be deployed at different distances from the spacecraft to determine an approximation of the interfering field for subsequent removal, but constant data streams from both magnetometers can be impractical due to power and telemetry limitations. Here we propose a method to identify and remove time-varying magnetic interference from sources such as reaction wheels using statistical decomposition and convolutional neural networks, providing high-fidelity magnetic field data even in cases where dual-sensor measurements are not constantly available. For example, a measurement interval from the Parker Solar Probe outboard magnetometer experienced a 95.1% reduction in reaction wheel interference following application of the proposed technique.

Statistical Decomposition and Machine Learning to Clean In-Situ Spaceflight Magnetic Field Measurements

M.G. Finley[1], T.A. Bowen[2], M. Pulupa[2], A. Koval[3,4], and D.M. Miles[1]

[1]Department of Physics and Astronomy, University of Iowa, IA, USA

[2]Space Sciences Laboratory, University of California, Berkeley, CA, USA

[3]Heliophysics Science Division, NASA, Goddard Space Flight Center, Greenbelt, MD, USA

[4]University of Maryland, Baltimore County, Baltimore, MD, USA

Corresponding author: Matthew G. Finley (matthew-g-finley@uiowa.edu)

Key Points:

- Local magnetic interference is a common issue faced by in-situ magnetometers.
- Gradiometer measurements have historically been required to denoise in-situ magnetometer data.
- Statistical decomposition and machine learning enable denoising even with limited gradiometer data.

Abstract

Robust in-situ magnetic field measurements are critical to understanding the various mechanisms that couple mass, momentum, and energy throughout our solar system. However, the spacecraft on which magnetometers are often deployed contaminate the magnetic field measurements via onboard subsystems including reaction wheels and magnetorquers. Two magnetometers can be deployed at different distances from the spacecraft to determine an approximation of the interfering field for subsequent removal, but constant data streams from both magnetometers can be impractical due to power and telemetry limitations. Here we propose a method to identify and remove time-varying magnetic interference from sources such as reaction wheels using statistical decomposition and convolutional neural networks, providing high-fidelity magnetic field data even in cases where dual-sensor measurements are not constantly available. For example, a measurement interval from the Parker Solar Probe outboard magnetometer experienced a 95.1% reduction in reaction wheel interference following application of the proposed technique.

Plain Language Summary

Measurements of magnetic fields captured by instruments onboard spacecraft are necessary to further our understanding of the solar system. These measurements are often contaminated by magnetic noise from the host spacecraft, substantially reducing the fidelity of the data. One common method to reduce the impact of these interfering magnetic fields utilizes a pair of magnetometers deployed at different distances from the main body of the spacecraft. The difference between the two sensors allows for an approximation of the interfering fields to be calculated for subsequent removal. However, many missions cannot afford to send data from both instruments back to Earth. This manuscript proposes a method for the mitigation of magnetic interference caused by the host spacecraft, even with limited data from the magnetometer pair. Specifically, signal decomposition techniques and machine learning are used to isolate and remove the interfering magnetic fields. For example, the proposed method applied to a measurement interval from the Parker Solar Probe outboard magnetometer enabled a 95% reduction in magnetic interference.

1 <u>Introduction</u>

High-quality in-situ magnetic field measurements are essential to understanding the geophysical processes that couple mass, energy, and momentum throughout near-Earth space and the solar system. This often involves identifying comparably small perturbations due to field-aligned currents or plasma processes from a much larger background field that, unfortunately, is often contaminated by magnetic noise from the host satellite platform. Stray magnetic fields can emanate from the materials used in the construction of the host spacecraft, from attitude control systems such as reaction wheels and magnetorquers, or from the solar panels, batteries, and electrical systems that manage power for the spacecraft subsystems.

To mitigate the impact of the interfering fields, magnetometers can be deployed on a boom, increasing the physical separation from the host spacecraft. Historically, very long booms (e.g., >5-meters) have been implemented to achieve optimal interference mitigation (Miller, 1979; Smola et al., 1980). For additional interference mitigation potential a pair of magnetometers has often been used, mounted at different distances along the boom. At a large distance from the source a simple dipole approximation can be fit to the field gradient and subtracted (Ness et al., 1971). However, many recent missions such as Van Allen Probes (Kletzing et al., 2013) and Dellingr (Clagett et al., 2017) have opted for shorter booms (3-meter and 0.52-meter, respectively) to reduce complexity and implementation costs. This reduced boom length tends to place the sensors in the near-field of the magnetic noise source where the complex multipole terms cannot be neglected. In theory, a multipole source model can still be used to subtract the gradient; however, this requires careful pre-flight characterization of all possible interference sources which can be challenging or logistically impossible.

Recently, additional techniques have been developed in order to mitigate local magnetic interference onboard spacecraft. One simple approach is to simply apply a band-stop filter at the frequencies associated with the dominant interference source (e.g., reaction wheels). However, methods that utilize this approach can encounter problems during spacecraft maneuvers, as the reaction wheels diverge from their nominal rates, contaminate extremely large frequency bands, and can spectrally overlap with geophysical signals of interest. Advanced methods such as blind source separation (Hoffmann & Moldwin, 2022; Sheinker & Moldwin, 2016), independent component analysis (Imajo et al., 2021), maximum variance analysis (Constantinescu et al., 2020), and spectrum-based feature extraction (Bowen, Mallet, et al., 2020) have been shown to successfully identify and remove interference from magnetometer measurements when two or more sensors are available without relying on hand-tuned filters.

Recent advances in machine learning techniques have seen their widespread adoption in various space physics fields. For example: Space weather forecasting (Camporeale, 2019), in-situ magnetometer calibration (Styp-Rekowski et al., 2022), auroral image classification (Clausen & Nickisch, 2018), and plasma modeling (Bard & Dorelli, 2021). These machine learning tools have been used in a variety of other fields in order to improve the fidelity of contaminated measurements (Tian et al., 2019; E. Wang & Nealon, 2019). However, interference mitigation for on-orbit magnetic field data utilizing machine learning techniques has not been thoroughly explored.

This manuscript proposes a novel method for the integration of machine learning and statistical decomposition for magnetometer interference mitigation. The proposed method leverages potentially limited gradiometer data and provides the capability to automatically identify and remove magnetic noise caused by the host spacecraft during intervals when only a single magnetometer is constantly telemetering data. For example, a measurement interval from only the Parker Solar Probe outboard magnetometer will be shown to experience a 95.1% reduction in interference attributed to the spacecraft's reaction wheels following the application of the proposed algorithm.

2 Methodology

2.1 *Statistical Decomposition and Classification for Gradiometers*

Singular Spectrum Analysis (SSA) is a statistical technique for the decomposition of signals into physical meaningful components (Golyandina et al., 2001; Groth & Ghil, 2015). Historically, this technique has seen success in a wide range of fields from climatology (Chen et al., 2013; Vautard & Ghil, 1989) to economics (Hassani et al., 2010; Hassani & Thomakos, 2010). Recently, the multivariate extension of SSA (MSSA) has been used to simultaneously decompose time-series measurements from a pair of satellite-mounted magnetometers into robust, physically meaningful components corresponding to the near-DC trend, interesting geomagnetic phenomena, and local magnetic interference (Finley et al., 2023).

Mathematically, this process can be defined as singular value decomposition (SVD) of a trajectory matrix (Groth & Ghil, 2015). The trajectory matrix is defined as

$$\boldsymbol{X} = \begin{bmatrix} x(1) & x(2) & \dots & x(K) \\ x(2) & x(3) & \dots & x(K+1) \\ \dots & \dots & \dots & \dots \\ x(L) & x(L+1) & \dots & x(N) \end{bmatrix}. \quad (1)$$

Note that $\boldsymbol{X}$, which is generated with columns as lagged copies of the original input, contains information about the temporal variation of the signal captured by the *window length*, L. Applying SVD determines the eigenvector matrix ($\boldsymbol{V}$) for the covariance matrix associated with the trajectory matrix (e.g., $\mathbf{XX}^{\mathrm{T}}$). The principal components of $\boldsymbol{X}$ can be determined by projecting it onto the eigenvectors via

$$\boldsymbol{P} = \boldsymbol{V}^T \boldsymbol{X}\,. \quad (\mathbf{2})$$

This process can then be inverted for each of the L principal components and associated eigenvectors. This is defined for each eigenvector V_i and principal component P_i as

$$\boldsymbol{R}_i = V_i \times P_i \; \forall i \in \{1, \dots, L\}. \quad (3)$$

The sub-signals, r_i, associated with each principal component are then calculated by averaging along the anti-diagonals of each of the L matrices $\boldsymbol{R}_i$. No information is lost in this process; summing all of the sub-signals will completely reconstruct the original input. The multichannel extension (MSSA) expands one dimension of the trajectory matrix by the number of channels such that spatiotemporal information from all inputs (e.g., measurements made by multiple magnetometers) is leveraged in the decomposition process.

Once the sub-signals have been calculated it is necessary to group them according to their apparent contribution to important geomagnetic phenomena or local magnetic interference generated by the host spacecraft so the interference can be removed. This is done by calculating the statistical correlation between the imperfect interference approximation provided by the magnetic field gradient,

$$\left(\hat{x}_{interference} = x_{inboard} - x_{outboard}\right), \quad (4)$$

and each of the decomposed sub-signals, r_i. A high degree of correlation implies that the sub-signals are morphologically similar to the interference approximation and should be removed. Setting a threshold parameter (α) subsequently determines the confidence of the interference mitigation algorithm and should be tuned accordingly. Further mathematical details and results for the application of this dual-sensor magnetometer denoising technique can be found in (Finley et al., 2023).

2.2 *Machine Learning for Single-Sensor Classification*

Although the field gradient between two magnetometers is useful in classifying decomposed sub-signals as geomagnetic phenomena or local interference, data is not always available from both magnetometers onboard a spacecraft. Often, telemetry limitations force compromises to be made when transmitting magnetic field data to the ground, resulting in limited intervals where two sensors are providing full-cadence measurements. This can obviously limit the applicability of the statistical interference mitigation technique described in Sec. 2.1 due to the unavailability of the interference approximation.

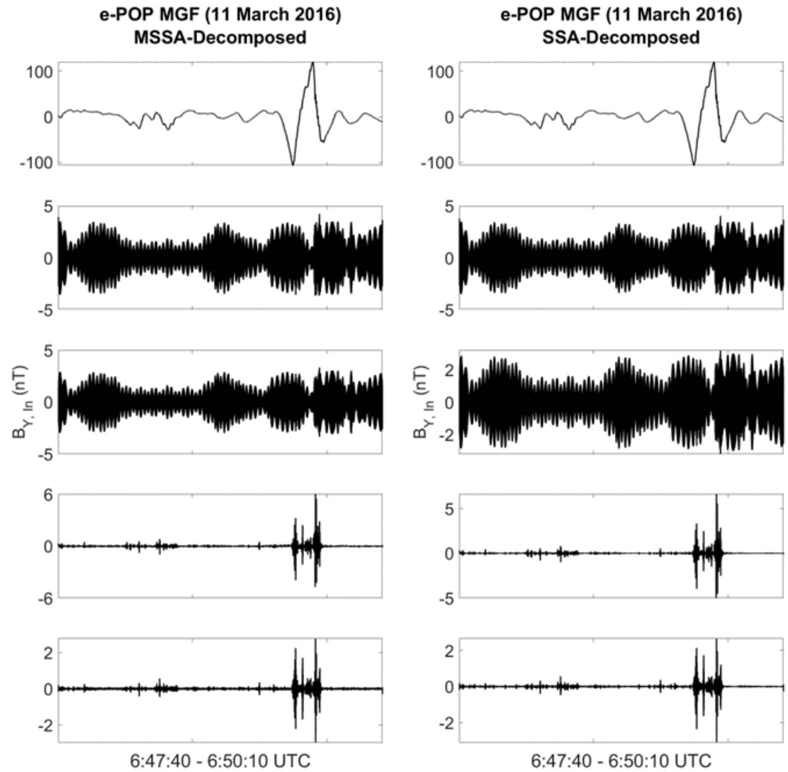

Figure 1: Inboard sensor sub-signals generated by applying MSSA to both sensors (left) and SSA applied only to the inboard sensor (right) on an interval of CASSIOPE/Swarm-Echo magnetic field data.

However, it can be observed that for well-synchronized and calibrated pairs of magnetometers, SSA and MSSA produce extremely similar results. Figure 1 illustrates the first five sub-signals output for the outboard sensor from the dual-sensor MSSA decomposition, as well as the single-sensor SSA decomposition for the outboard sensor, over an interval of CASSIOPE/Swarm-Echo magnetic field data (Wallis et al., 2015; Yau & James, 2015). Note that the same features such as near-DC trend (Row 1), oscillations presumably caused by reaction wheels (Rows 2 and 3), and geomagnetic phenomena (Rows 4 and 5) previously identified as Alfvénic activity (Finley et al., 2023; Miles et al., 2018) can be seen in both methods of decomposition. This implies that the classification of the sub-signals decomposed by both techniques should also be extremely similar, although we cannot rely on the simple field gradient for classification when only one sensor is available.

Recent advances in machine learning (ML) tools have seen neural networks achieve a great deal of success in classifying time-series signals. This manuscript proposes the use of such networks to automatically classify signals decomposed by SSA as either local magnetic interference or residual geophysical signal, enabling interference mitigation even when only a single magnetometer is constantly telemetering data. A high-level block diagram of the proposed technique is shown in Fig. 2a. During intervals where two magnetic field sensors are telemetering data, MSSA is used to decompose the measurements and the magnetic gradient between the sensors is used to classify them, as explained in Sec. 2.1(Finley et al., 2023). These decomposed signals and associated labels are used to train a Convolutional Neural Network (CNN), which is used to perform the same binary classification on SSA-decomposed signals when measurements from only a single magnetometer are available.

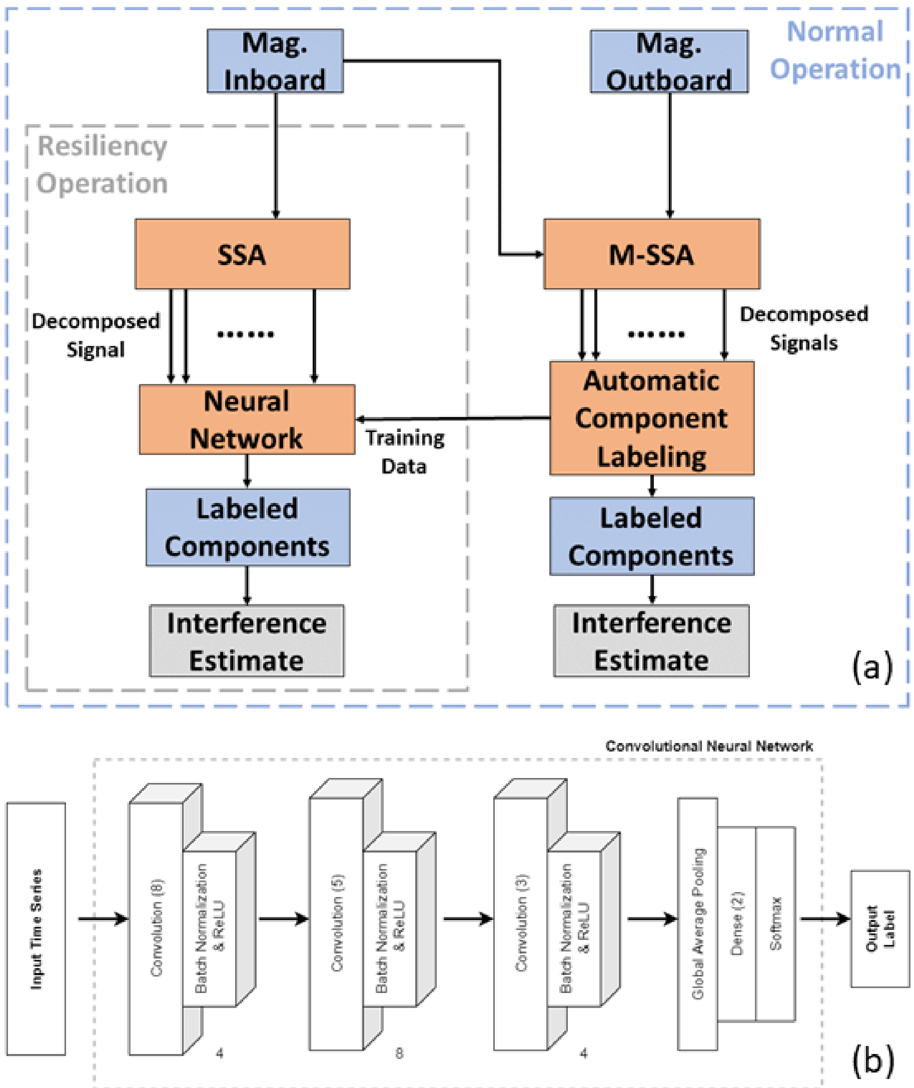

Figure 2: Illustration of the proposed method of interference mitigation applicable to intervals where only a single magnetic field sensor is available. (a) High-level block diagram of proposed method; (b) Specific CNN utilized by the proposed method.

The specific CNN implemented for this manuscript is shown in Fig. 2b, and was adapted from a similar architecture described in (Z. Wang et al., 2017). This network was selected due to the simplicity of its implementation and its performance history on classification of time series data. The basic building block of this network is a convolutional layer followed by batch normalization and the *ReLU* activation function to provide nonlinearity. The filter applied at each convolution decreases in length from eight to five to three for each of the respective blocks. The number of filters applied in each convolutional layer is four for the leftmost and rightmost block, and is eight at the center block. After the convolutions are applied, a global pooling operation is performed, a dense layer is used to adjust the dimensionality, and the *Softmax* activation function provides the probability associated with the binary output labels. This network was implemented in MATLAB 2022b using functionality from the Deep Learning Toolbox. Training parameters and results are discussed in detail in Sec. 4.

3 Data

3.1 *CASSIOPE e-POP/Swarm-Echo MGF*

The first source of data analyzed in this manuscript is from the CASSIOPE/Swarm-Echo magnetic field instrument (MGF). These identical fluxgate magnetometers are deployed on a common boom at distances of approximately 0.9 and 0.6 meters from the host spacecraft. Both sensors measure and telemeter data at a cadence of 160 Sa/sec. The specific intervals chosen for visualization or analysis were selected due to the presence of interesting geophysical events such as the Alfvén waves (Miles et al., 2018) shown in Fig. 1 and ion downflow (Shen et al., 2016, 2018) shown in Sec. 4. Note that a 20-sec mean has been removed from the original measurements captured by the e-POP MGF for ease of visualization.

3.2 *Parker Solar Probe FIELDS MAG*

Another source of data analyzed in this manuscript is from the Parker Solar Probe/FIELDS experiment (Bale et al., 2016). FIELDS consists of two fluxgate magnetometers (MAGs) 1.9 and 2.7 m from the spacecraft, which operate at a maximum sample rate of 292.969 Sa/sec (Bowen, Bale, et al., 2020). The dual sensors provide for failure redundancy, gradiometric estimates of spacecraft noise, and monitoring of variations in DC offsets. The outboard MAG (MAGo) is less impacted by spacecraft noise and accordingly used as the primary science instrument. The inboard MAG (MAGi) is generally run at a lower sample cadence due to telemetry constraints of the mission. Data chosen in this study were chosen due to the identical sample rates of the inboard and outboard measurements. Note that low-frequency interference from other subsystems dominates the field gradient spectrum, and a high-pass filter at 3 Hz is applied to enable isolation of only the reaction wheels, which are a significant source of noise in studying the polarization of plasma waves (Bowen, Mallet, et al., 2020).

4 Results

4.1 *Neural Network Training*

The CNN used to classify decomposed sub-signals on e-POP MGF data was trained using gradiometer data from 1-5 March 2016. The data was split into 40-second intervals (i.e., 6400 samples/interval) and discarded if NaN values were present in either the inboard or outboard measurements (due to data dropouts or other factors). Each of the resulting 476 pairs of measurements were passed through MSSA with a window length of 40, resulting in ~39,000 pairs of sub-signals that were subsequently labeled via correlation against the magnetic field gradient with a threshold of 0.55. This threshold value was intentionally set high to increase the confidence in the labeling scheme, although the resulting labels may still be incorrect when the statistical significance of the sub-signals is ambiguous. Of the original ~76,000 sub-signals, ~2,500 were labeled as interference and ~74,000 were labeled as residual geophysical signal. A random permutation of 2,000 of the sub-signals corresponding to each binary label were selected as inputs to the CNN training.

A similar data processing scheme was utilized for the limited gradiometer data from the Parker Solar Probe MAG. Only three hours of data (06:00:00 – 09:00:00 UTC) from 30 March 2019 (Encounter 2) were processed with a window length of 40 and a threshold value of 0.35, resulting in ~43,000 labeled 40-second intervals (~2,600 labeled as local interference, ~40,500 labeled as residual geophysical signal). A random permutation of 2,500 of the sub-signals corresponding to each label were selected as inputs to the CNN training.

Prior to training the CNN, all input data were normalized between 0 and 1. The total input set was divided randomly into training, validation, and testing sub-sets using a typical 80%, 10%, 10% split. The network was then trained, using the default Adam optimizer (Kingma & Ba, 2017) to minimize the cross-entropy loss function, for ten epochs. Cross-entropy, which calculates the difference between two probability distributions, is a standard choice for classification networks (de Boer et al., 2005). It is important to note that, given the potential for misclassification in the generation of the training set, the performance of the classification network is not necessarily indicative of the performance of the interference mitigation algorithm as a whole. That said, the CNN trained on e-POP MGF data achieved a validation accuracy and loss of 98.0% and 0.086. The CNN trained on PSP MAG data achieved a validation accuracy and loss of 98.86% and 0.046.

4.2 *Numerical Analysis*

To quantitatively assess the performance of the proposed method in mitigating stray magnetic field caused by reaction wheels, it is necessary to perform numerical analysis of the results. This manuscript calculates the linear spectrum associated with the apparent reaction wheel frequencies during the events under observation before and after the application of the proposed method of single-sensor decomposition and ML-enabled sub-signal classification. Results are also calculated for the dual-sensor, gradient-based algorithm to provide a comparison with the technique used to train the classification network.

The values of the linear spectrum associated with the reaction wheel frequencies is calculated using Welch's method of overlapping periodograms (Welch, 1967) and an HFT95 flat-top window with an effective noise bandwidth (ENBW) of 3.8112 Hz (Heinzel et al., 2002). Mathematically, the linear spectrum (LS) can be defined based on the power spectral density (PSD) resulting from Welch's method as

$$LS = \sqrt{PSD \times ENBW}. \tag{5}$$

The results analyzed in this section are from data with near-constant reaction wheel rates for computational simplicity in the absence of a ground truth. Note that, during the intervals selected for analysis, the CASSIOPE reaction wheels were spinning at a uniform rate. As such, only one frequency point must be analyzed to determine the mitigation performance provided by the proposed method. However, the Parker Solar Probe reaction wheels are not at a uniform rate during these intervals, so the linear spectrum value attributed to each reaction wheel frequency (determined using the spacecraft's housekeeping data) is calculated and averaged.

4.3 *Experiments*

The proposed method of automated single-sensor interference mitigation utilizing machine learning classification techniques was applied to four distinct intervals of magnetometer data from two different missions, as shown in Fig. 3. Each row of Fig. 3 corresponds to one interval: Row 1 and 2 illustrate the proposed method applied e-POP MGF data during ion downflow events (Shen et al., 2016, 2018); Row 3 and 4 illustrate the technique applied to intervals of Parker Solar Probe (PSP) MAG data during Encounter 2. The first two columns of Fig. 3 show the outboard measurements before and after the single-sensor correction, as well as after the dual-sensor correction for comparison. Column 1 shows the entire 40-second interval under observation, whereas Column 2 shows a 2-second zoomed view for ease of visualization. Columns 3-5 show the spectra associated with the uncorrected, single-sensor corrected, and dual-sensor corrected measurements, respectively. The red dashed lines overlaid on the spectra correspond to the frequencies of the spacecraft's reaction wheels during these intervals, although this information is not required in the implementation of the proposed interference mitigation technique.

Table 1 provides numerical results for the proposed interference mitigation method using the analysis technique described in Sec. 4.2. The specific frequencies analyzed correspond to the dashed red lines overlaid on the spectra in Fig. 3. For the e-POP MGF events shown, the proposed single-sensor method reduces the amplitude of the frequencies associated with the spacecraft reaction wheels by greater than 87%. For the PSP MAG intervals during Encounter 2, an amplitude reduction of greater than 95% can be seen.

These results are compared to the dual-sensor interference mitigation method, which utilized the same window length (L = 40) as in the single-sensor decomposition, paired with a threshold value of 0.25 for PSP and 0.15 for e-POP. Amplitude reductions of greater than 88% and 78% can be seen for e-POP and PSP, respectively. This slightly lower reduction (specifically for the PSP MAG) can be attributed to the substantial time-frequency overlap seen between the apparent reaction wheel interference and the observed magnetic phenomena during the intervals analyzed.

As the SSA technique and its multivariate extension provide asymptotic separability (Harmouche et al., 2018), larger window lengths enable signal elements with close spectral signatures to be decomposed from one another; however, greater window length also increases the number of sub-signals generated by the decomposition, potentially reducing their statistical significance. As such, an identical window length was used across all experiments for simplicity and consistency. Qualitative analysis of the results displayed in Fig. 3 corroborate this assessment: although both single-sensor and dual-sensor interference mitigation techniques substantially reduce the power at the reaction wheel frequencies, the single-sensor method negates a slightly larger bandwidth surrounding the apparent reaction wheel signature. Although this results in higher numerical accuracy, it is not necessarily indicative of better algorithm performance, and is instead likely an artifact of the limited training set provided to the CNN. More robust models utilizing all available gradiometer data, hyperparameter optimization, and model generalizability across missions are all exciting avenues for future work related to the proposed method of interference mitigation.

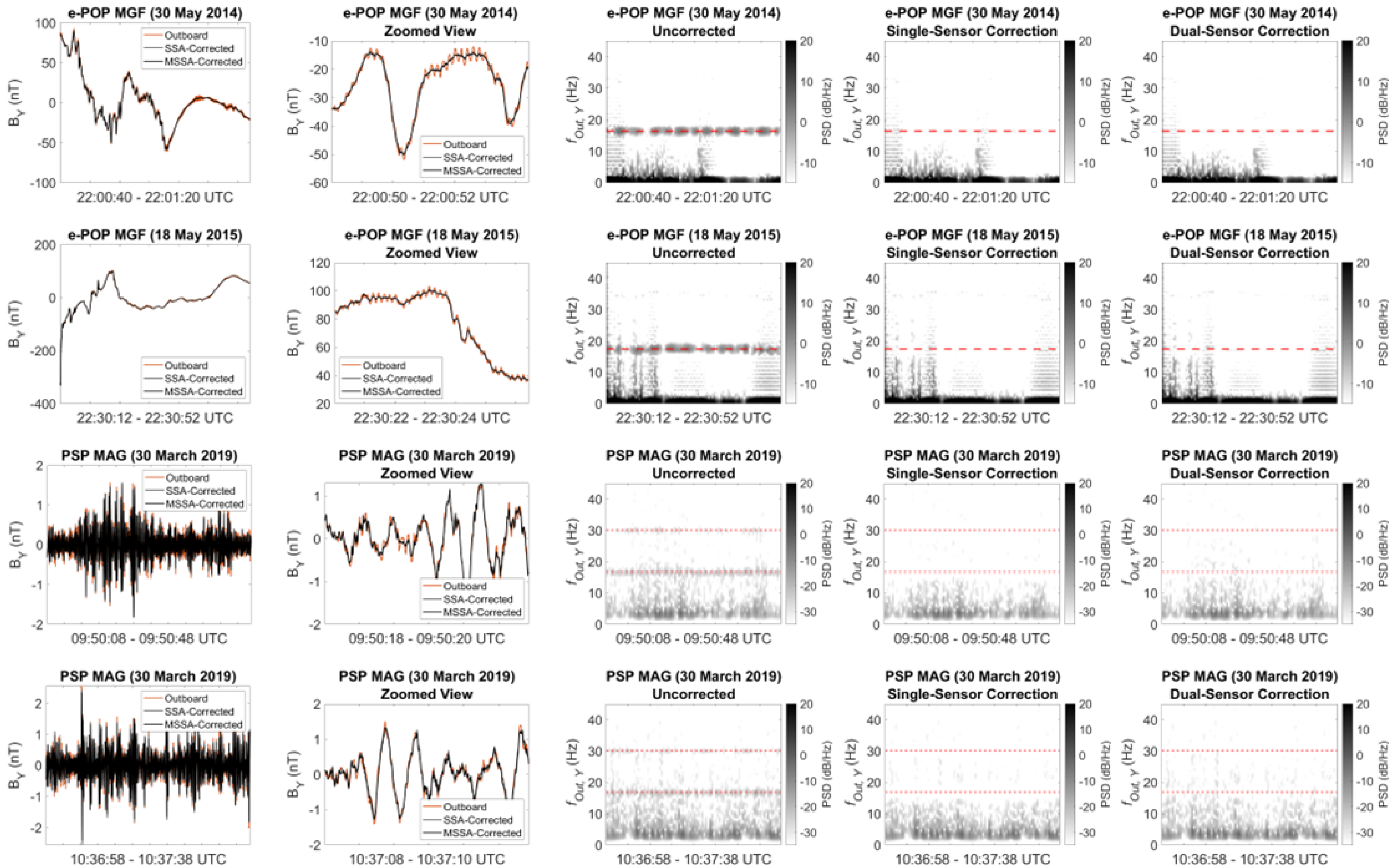

Figure 3: The proposed method of single-sensor interference mitigation compared to dual-sensor mitigation during intervals of e-POP MGF data captured during geomagnetic phenomena (Rows 1-2) and Parker Solar Probe MAG data captured during Encounter 2 (Rows 3-4). (Columns 1-2) Forty-second total interval and two-second zoomed interval time-series data for uncorrected, single-sensor corrected, and dual-sensor corrected outboard measurements; (Column 3) Uncorrected outboard spectrum; (Column 4) Single-sensor corrected outboard spectrum; (Column 5) Dual-sensor corrected outboard spectrum. The dashed red lines indicate the reaction wheel frequencies during each interval.

Table 1: Numerical analysis for the events shown in Fig. 3. (Rows 1-2) Results for interesting geomagnetic intervals captured by the e-POP MGF; (Rows 3-4) Results for PSP MAG data captured during Encounter 2.

	Event	**Dominant Wheel Tones**	**Uncorrected** (Linear Spectrum)	**SSA-Corrected** (Linear Spectrum)	**SSA-Corrected** (Improvement)	**MSSA-Corrected** (Linear Spectrum)	**MSSA-Corrected** (Improvement)
e-POP MGF	**30 May 2014 (22:00:40 UTC)**	16.4 Hz (x4)	1.18 nT	0.15 nT	87.2%	0.04 nT	96.6%
	18 May 2015 (22:30:12 UTC)	17.5 Hz (x4)	0.98 nT	0.07 nT	92.8%	0.11 nT	88.7%
PSP MAG	**30 March 2019 (9:50:08 UTC)**	16.4 Hz, 17.1 Hz, 29.9 Hz, 30.0 Hz	0.042 nT	0.002 nT	95.2%	0.009 nT	78.5%
	30 March 2019 (10:36:58 UTC)	16.6 Hz, 17.1 Hz, 30.0 Hz, 30.1 Hz	0.041 nT	0.002 nT	95.1%	0.007 nT	82.9%

5 Conclusions

This manuscript has presented a novel method for the automatic mitigation of local magnetic interference from sources such as reaction wheels on spacecraft where gradiometer measurements are not always available. Specifically, statistical decomposition and analysis provide a large dataset of labeled sub-signals when gradiometer measurements are available. This dataset is subsequently used to train a neural network to label decomposed signals as local interference or residual physical fields when data from only a single magnetometer is available. This method has been tested, with positive results, against measurements from the CASSIOPE/Swarm-Echo and Parker Solar Probe missions. For example, on a 40-second interval of data during Parker Solar Probe's Encounter 2, a reduction in reaction wheel amplitude of 95.2% can be seen following the application of the proposed method.

Acknowledgments

The CASSIOPE/Swarm-Echo mission is supported by the European Space Agency's Third Party Mission Program. This work was supported in part by the US Air Force Office of Scientific Research (FA9550-21-1-0206). Parker Solar Probe was designed, built, and is now operated by the Johns Hopkins Applied Physics Laboratory as part of NASA's Living With a Star (LWS) program (contract NNN06AA01C).

Open Research

All CASSIOPE/Swarm-Echo MGF data, including the examples used in this manuscript, is publicly available at https://epop-data.phys.ucalgary.ca/. Public access to outboard measurements from Parker Solar Probe MAG is available at https://fields.ssl.berkeley.edu/data/. The Parker Solar Probe MAG inboard data used in this manuscript, as well as the code and data used to generate the figures and analysis, are currently stored at https://iowa-my.sharepoint.com/:f:/g/personal/mgfinley_uiowa_edu/ErDxXKn5NSRGuRP6UqP3050Bm4Vq68Njb3L1dClgfK2ROg. Upon acceptance of this manuscript the code and data will be stored in a University of Iowa Institutional Repository for long-term storage and reuse.

References

Bale, S. D., Goetz, K., Harvey, P. R., Turin, P., Bonnell, J. W., Dudok de Wit, T., Ergun, R. E., MacDowall, R. J., Pulupa, M., Andre, M., Bolton, M., Bougeret, J.-L., Bowen, T. A., Burgess, D., Cattell, C. A., Chandran, B. D. G., Chaston, C. C., Chen, C. H. K., Choi, M. K., … Wygant, J. R. (2016). The FIELDS Instrument Suite for Solar Probe Plus. *Space Science Reviews*, *204*(1), 49–82. https://doi.org/10.1007/s11214-016-0244-5

Bard, C., & Dorelli, J. C. (2021). Neural Network Reconstruction of Plasma Space-Time. *Frontiers in Astronomy and Space Sciences*, *8*. https://www.frontiersin.org/articles/10.3389/fspas.2021.732275

Bowen, T. A., Bale, S. D., Bonnell, J. W., Dudok de Wit, T., Goetz, K., Goodrich, K., Gruesbeck, J., Harvey, P. R., Jannet, G., Koval, A., MacDowall, R. J., Malaspina, D. M., Pulupa, M., Revillet, C., Sheppard, D., & Szabo, A. (2020). A Merged Search-Coil and Fluxgate Magnetometer Data Product for Parker Solar Probe FIELDS. *Journal of Geophysical Research: Space Physics*, *125*(5), e2020JA027813. https://doi.org/10.1029/2020JA027813

Bowen, T. A., Mallet, A., Huang, J., Klein, K. G., Malaspina, D. M., Stevens, M., Bale, S. D., Bonnell, J. W., Case, A. W., Chandran, B. D. G., Chaston, C. C., Chen, C. H. K., Dudok de Wit, T., Goetz, K., Harvey, P. R., Howes, G. G., Kasper, J. C., Korreck, K. E., Larson, D., … The PSP/FIELDS and PSP/SWEAP Teams. (2020). Ion-scale Electromagnetic Waves in the Inner Heliosphere. *The Astrophysical Journal Supplement Series*, *246*(2), 66. https://doi.org/10.3847/1538-4365/ab6c65

Camporeale, E. (2019). The Challenge of Machine Learning in Space Weather: Nowcasting and Forecasting. *Space Weather*, *17*(8), 1166–1207. https://doi.org/10.1029/2018SW002061

Chen, Q., van Dam, T., Sneeuw, N., Collilieux, X., Weigelt, M., & Rebischung, P. (2013). Singular spectrum analysis for modeling seasonal signals from GPS time series. *Journal of Geodynamics*, *72*, 25–35. https://doi.org/10.1016/j.jog.2013.05.005

Clagett, C., Santos, L., Azimi, B., Cudmore, A., Marshall, J., Starin, S., Sheikh, S., Zesta, E., Paschalidis, N., Johnson, M., Kepko, L., Berry, D., Bonalsky, T., Chai, D., Colvin, M., Evans, A., Hesh, S., Jones, S., Peterson, Z., … Rodriquez, M. (2017). Dellingr: NASA

Goddard Space Flight Center's First 6U Spacecraft. *Small Satellite Conference*. https://digitalcommons.usu.edu/smallsat/2017/all2017/83

Clausen, L. B. N., & Nickisch, H. (2018). Automatic Classification of Auroral Images From the Oslo Auroral THEMIS (OATH) Data Set Using Machine Learning. *Journal of Geophysical Research: Space Physics*, *123*(7), 5640–5647. https://doi.org/10.1029/2018JA025274

Constantinescu, O. D., Auster, H.-U., Delva, M., Hillenmaier, O., Magnes, W., & Plaschke, F. (2020). Maximum-variance gradiometer technique for removal of spacecraft-generated disturbances from magnetic field data. *Geoscientific Instrumentation, Methods and Data Systems*, *9*(2), 451–469. https://doi.org/10.5194/gi-9-451-2020

de Boer, P.-T., Kroese, D. P., Mannor, S., & Rubinstein, R. Y. (2005). A Tutorial on the Cross-Entropy Method. *Annals of Operations Research*, *134*(1), 19–67. https://doi.org/10.1007/s10479-005-5724-z

Finley, M. G., Broadfoot, R. M., Shekhar, S., & Miles, D. M. (2023). Identification and Removal of Reaction Wheel Interference From In-Situ Magnetic Field Data Using Multichannel Singular Spectrum Analysis. *Journal of Geophysical Research: Space Physics*, *128*(2), e2022JA031020. https://doi.org/10.1029/2022JA031020

Golyandina, N., Nekrutkin, V., & Zhigljavsky, A. A. (2001). *Analysis of Time Series Structure: SSA and Related Techniques*. CRC Press.

Groth, A., & Ghil, M. (2015). Monte Carlo Singular Spectrum Analysis (SSA) Revisited: Detecting Oscillator Clusters in Multivariate Datasets. *Journal of Climate*, *28*(19), 7873–7893. https://doi.org/10.1175/JCLI-D-15-0100.1

Harmouche, J., Fourer, D., Auger, F., Borgnat, P., & Flandrin, P. (2018). The Sliding Singular Spectrum Analysis: A Data-Driven Nonstationary Signal Decomposition Tool. *IEEE Transactions on Signal Processing*, *66*(1), 251–263. https://doi.org/10.1109/TSP.2017.2752720

Hassani, H., Soofi, A. S., & Zhigljavsky, A. A. (2010). Predicting daily exchange rate with singular spectrum analysis. *Nonlinear Analysis: Real World Applications*, *11*(3), 2023–2034. https://doi.org/10.1016/j.nonrwa.2009.05.008

Hassani, H., & Thomakos, D. (2010). A review on singular spectrum analysis for economic and financial time series. *Statistics and Its Interface*, *3*(3), 377–397. https://doi.org/10.4310/SII.2010.v3.n3.a11

Heinzel, G., Rudiger, A., & Schilling, R. (2002). *Spectrum and spectral density estimation by the Discrete Fourier transform (DFT), including a comprehensive list of window functions and some new flat-top windows.*

Hoffmann, A. P., & Moldwin, M. B. (2022). Separation of Spacecraft Noise From Geomagnetic Field Observations Through Density-Based Cluster Analysis and Compressive Sensing. *Journal of Geophysical Research: Space Physics*, *127*(9), e2022JA030757. https://doi.org/10.1029/2022JA030757

Imajo, S., Nosé, M., Aida, M., Matsumoto, H., Higashio, N., Tokunaga, T., & Matsuoka, A. (2021). Signal and Noise Separation From Satellite Magnetic Field Data Through Independent Component Analysis: Prospect of Magnetic Measurements Without Boom and Noise Source Information. *Journal of Geophysical Research: Space Physics*, *126*(5), e2020JA028790. https://doi.org/10.1029/2020JA028790

Kingma, D. P., & Ba, J. (2017). *Adam: A Method for Stochastic Optimization* (arXiv:1412.6980). arXiv. https://doi.org/10.48550/arXiv.1412.6980

Kletzing, C. A., Kurth, W. S., Acuna, M., MacDowall, R. J., Torbert, R. B., Averkamp, T., Bodet, D., Bounds, S. R., Chutter, M., Connerney, J., Crawford, D., Dolan, J. S., Dvorsky, R., Hospodarsky, G. B., Howard, J., Jordanova, V., Johnson, R. A., Kirchner, D. L., Mokrzycki, B., … Tyler, J. (2013). The Electric and Magnetic Field Instrument Suite and Integrated Science (EMFISIS) on RBSP. *Space Science Reviews*, *179*(1), 127–181. https://doi.org/10.1007/s11214-013-9993-6

Miles, D. M., Mann, I. R., Pakhotin, I. P., Burchill, J. K., Howarth, A. D., Knudsen, D. J., Lysak, R. L., Wallis, D. D., Cogger, L. L., & Yau, A. W. (2018). Alfvénic Dynamics and Fine Structuring of Discrete Auroral Arcs: Swarm and e-POP Observations. *Geophysical Research Letters*, *45*(2), 545–555. https://doi.org/10.1002/2017GL076051

Miller, D. C. (1979, April 1). *The Voyager magnetometer boom*. https://ntrs.nasa.gov/citations/19790013187

Ness, N. F., Behannon, K. W., Lepping, R. P., & Schatten, K. H. (1971). Use of two magnetometers for magnetic field measurements on a spacecraft. *Journal of Geophysical Research (1896-1977)*, *76*(16), 3564–3573. https://doi.org/10.1029/JA076i016p03564

Sheinker, A., & Moldwin, M. B. (2016). Adaptive interference cancelation using a pair of magnetometers. *IEEE Transactions on Aerospace and Electronic Systems*, *52*(1), 307–318. https://doi.org/10.1109/TAES.2015.150192

Shen, Y., Knudsen, D. J., Burchill, J. K., Howarth, A. D., Yau, A. W., Miles, D. M., James, H. G., Perry, G. W., & Cogger, L. (2018). Low-Altitude Ion Heating, Downflowing Ions, and BBELF Waves in the Return Current Region. *Journal of Geophysical Research: Space Physics*, *123*(4), 3087–3110. https://doi.org/10.1002/2017JA024955

Shen, Y., Knudsen, D. J., Burchill, J. K., Howarth, A., Yau, A., Redmon, R. J., Miles, D. M., Varney, R. H., & Nicolls, M. J. (2016). Strong ambipolar-driven ion upflow within the cleft ion fountain during low geomagnetic activity. *Journal of Geophysical Research: Space Physics*, *121*(7), 6950–6969. https://doi.org/10.1002/2016JA022532

Smola, J. F., Radford, W. E., & Reitz, M. H. (1980, May 1). *The Magsat magnetometer boom*. https://ntrs.nasa.gov/citations/19800015026

Styp-Rekowski, K., Michaelis, I., Stolle, C., Baerenzung, J., Korte, M., & Kao, O. (2022). Machine learning-based calibration of the GOCE satellite platform magnetometers. *Earth, Planets and Space*, *74*(1), 138. https://doi.org/10.1186/s40623-022-01695-2

Tian, C., Xu, Y., Fei, L., & Yan, K. (2019). Deep Learning for Image Denoising: A Survey. In J.-S. Pan, J. C.-W. Lin, B. Sui, & S.-P. Tseng (Eds.), *Genetic and Evolutionary Computing* (pp. 563–572). Springer. https://doi.org/10.1007/978-981-13-5841-8_59

Vautard, R., & Ghil, M. (1989). Singular spectrum analysis in nonlinear dynamics, with applications to paleoclimatic time series. *Physica D: Nonlinear Phenomena*, *35*(3), 395–424. https://doi.org/10.1016/0167-2789(89)90077-8

Wallis, D. D., Miles, D. M., Narod, B. B., Bennest, J. R., Murphy, K. R., Mann, I. R., & Yau, A. W. (2015). The CASSIOPE/e-POP Magnetic Field Instrument (MGF). *Space Science Reviews*, *189*(1), 27–39. https://doi.org/10.1007/s11214-014-0105-z

Wang, E., & Nealon, J. (2019). Applying machine learning to 3D seismic image denoising and enhancement. *Interpretation*, *7*(3), SE131–SE139. https://doi.org/10.1190/INT-2018-0224.1

Wang, Z., Yan, W., & Oates, T. (2017). Time series classification from scratch with deep neural networks: A strong baseline. *2017 International Joint Conference on Neural Networks (IJCNN)*, 1578–1585. https://doi.org/10.1109/IJCNN.2017.7966039

Welch, P. (1967). The use of fast Fourier transform for the estimation of power spectra: A method based on time averaging over short, modified periodograms. *IEEE Transactions on Audio and Electroacoustics*, *15*(2), 70–73. https://doi.org/10.1109/TAU.1967.1161901

Yau, A. W., & James, H. G. (2015). CASSIOPE Enhanced Polar Outflow Probe (e-POP) Mission Overview. *Space Science Reviews*, *189*(1), 3–14. https://doi.org/10.1007/s11214-015-0135-1

Statistical Decomposition and Machine Learning to Clean In-Situ Spaceflight Magnetic Field Measurements

M.G. Finley[1], T.A. Bowen[2], M. Pulupa[2], A. Koval[3,4], and D.M. Miles[1]

[1]Department of Physics and Astronomy, University of Iowa, IA, USA

[2]Space Sciences Laboratory, University of California, Berkeley, CA, USA

[3]Heliophysics Science Division, NASA, Goddard Space Flight Center, Greenbelt, MD, USA

[4]University of Maryland, Baltimore County, Baltimore, MD, USA

Corresponding author: Matthew G. Finley (matthew-g-finley@uiowa.edu)

Key Points:

- Local magnetic interference is a common issue faced by in-situ magnetometers.
- Gradiometer measurements have historically been required to denoise in-situ magnetometer data.
- Statistical decomposition and machine learning enable denoising even with limited gradiometer data.

Abstract

Robust in-situ magnetic field measurements are critical to understanding the various mechanisms that couple mass, momentum, and energy throughout our solar system. However, the spacecraft on which magnetometers are often deployed contaminate the magnetic field measurements via onboard subsystems including reaction wheels and magnetorquers. Two magnetometers can be deployed at different distances from the spacecraft to determine an approximation of the interfering field for subsequent removal, but constant data streams from both magnetometers can be impractical due to power and telemetry limitations. Here we propose a method to identify and remove time-varying magnetic interference from sources such as reaction wheels using statistical decomposition and convolutional neural networks, providing high-fidelity magnetic field data even in cases where dual-sensor measurements are not constantly available. For example, a measurement interval from the Parker Solar Probe outboard magnetometer experienced a 95.1% reduction in reaction wheel interference following application of the proposed technique.

Plain Language Summary

Measurements of magnetic fields captured by instruments onboard spacecraft are necessary to further our understanding of the solar system. These measurements are often contaminated by magnetic noise from the host spacecraft, substantially reducing the fidelity of the data. One common method to reduce the impact of these interfering magnetic fields utilizes a pair of magnetometers deployed at different distances from the main body of the spacecraft. The difference between the two sensors allows for an approximation of the interfering fields to be calculated for subsequent removal. However, many missions cannot afford to send data from both instruments back to Earth. This manuscript proposes a method for the mitigation of magnetic interference caused by the host spacecraft, even with limited data from the magnetometer pair. Specifically, signal decomposition techniques and machine learning are used to isolate and remove the interfering magnetic fields. For example, the proposed method applied to a measurement interval from the Parker Solar Probe outboard magnetometer enabled a 95% reduction in magnetic interference.

1 Introduction

High-quality in-situ magnetic field measurements are essential to understanding the geophysical processes that couple mass, energy, and momentum throughout near-Earth space and the solar system. This often involves identifying comparably small perturbations due to field-aligned currents or plasma processes from a much larger background field that, unfortunately, is often contaminated by magnetic noise from the host satellite platform. Stray magnetic fields can emanate from the materials used in the construction of the host spacecraft, from attitude control systems such as reaction wheels and magnetorquers, or from the solar panels, batteries, and electrical systems that manage power for the spacecraft subsystems.

To mitigate the impact of the interfering fields, magnetometers can be deployed on a boom, increasing the physical separation from the host spacecraft. Historically, very long booms (e.g., >5-meters) have been implemented to achieve optimal interference mitigation (Miller, 1979; Smola et al., 1980). For additional interference mitigation potential a pair of magnetometers has often been used, mounted at different distances along the boom. At a large distance from the source a simple dipole approximation can be fit to the field gradient and subtracted (Ness et al., 1971). However, many recent missions such as Van Allen Probes (Kletzing et al., 2013) and Dellingr (Clagett et al., 2017) have opted for shorter booms (3-meter and 0.52-meter, respectively) to reduce complexity and implementation costs. This reduced boom length tends to place the sensors in the near-field of the magnetic noise source where the complex multipole terms cannot be neglected. In theory, a multipole source model can still be used to subtract the gradient; however, this requires careful pre-flight characterization of all possible interference sources which can be challenging or logistically impossible.

Recently, additional techniques have been developed in order to mitigate local magnetic interference onboard spacecraft. One simple approach is to simply apply a band-stop filter at the frequencies associated with the dominant interference source (e.g., reaction wheels). However, methods that utilize this approach can encounter problems during spacecraft maneuvers, as the reaction wheels diverge from their nominal rates, contaminate extremely large frequency bands, and can spectrally overlap with geophysical signals of interest. Advanced methods such as blind source separation (Hoffmann & Moldwin, 2022; Sheinker & Moldwin, 2016), independent component analysis (Imajo et al., 2021), maximum variance analysis (Constantinescu et al., 2020), and spectrum-based feature extraction (Bowen, Mallet, et al., 2020) have been shown to successfully identify and remove interference from magnetometer measurements when two or more sensors are available without relying on hand-tuned filters.

Recent advances in machine learning techniques have seen their widespread adoption in various space physics fields. For example: Space weather forecasting (Camporeale, 2019), in-situ magnetometer calibration (Styp-Rekowski et al., 2022), auroral image classification (Clausen & Nickisch, 2018), and plasma modeling (Bard & Dorelli, 2021). These machine learning tools have been used in a variety of other fields in order to improve the fidelity of contaminated measurements (Tian et al., 2019; E. Wang & Nealon, 2019). However, interference mitigation for on-orbit magnetic field data utilizing machine learning techniques has not been thoroughly explored.

This manuscript proposes a novel method for the integration of machine learning and statistical decomposition for magnetometer interference mitigation. The proposed method leverages potentially limited gradiometer data and provides the capability to automatically identify and remove magnetic noise caused by the host spacecraft during intervals when only a single magnetometer is constantly telemetering data. For example, a measurement interval from only the Parker Solar Probe outboard magnetometer will be shown to experience a 95.1% reduction in interference attributed to the spacecraft's reaction wheels following the application of the proposed algorithm.

2 <u>Methodology</u>

2.1 *Statistical Decomposition and Classification for Gradiometers*

Singular Spectrum Analysis (SSA) is a statistical technique for the decomposition of signals into physical meaningful components (Golyandina et al., 2001; Groth & Ghil, 2015). Historically, this technique has seen success in a wide range of fields from climatology (Chen et al., 2013; Vautard & Ghil, 1989) to economics (Hassani et al., 2010; Hassani & Thomakos, 2010). Recently, the multivariate extension of SSA (MSSA) has been used to simultaneously decompose time-series measurements from a pair of satellite-mounted magnetometers into robust, physically meaningful components corresponding to the near-DC trend, interesting geomagnetic phenomena, and local magnetic interference (Finley et al., 2023).

Mathematically, this process can be defined as singular value decomposition (SVD) of a trajectory matrix (Groth & Ghil, 2015). The trajectory matrix is defined as

$$\boldsymbol{X} = \begin{bmatrix} x(1) & x(2) & \dots & x(K) \\ x(2) & x(3) & \dots & x(K+1) \\ \dots & \dots & \dots & \dots \\ x(L) & x(L+1) & \dots & x(N) \end{bmatrix}. \quad (1)$$

Note that $\boldsymbol{X}$, which is generated with columns as lagged copies of the original input, contains information about the temporal variation of the signal captured by the *window length*, *L*. Applying SVD determines the eigenvector matrix ($\boldsymbol{V}$) for the covariance matrix associated with the trajectory matrix (e.g., $\mathbf{XX}^{\mathrm{T}}$). The principal components of $\boldsymbol{X}$ can be determined by projecting it onto the eigenvectors via

$$\boldsymbol{P} = \boldsymbol{V}^T \boldsymbol{X}\,. \quad (\mathbf{2})$$

This process can then be inverted for each of the L principal components and associated eigenvectors. This is defined for each eigenvector V_i and principal component P_i as

$$\boldsymbol{R}_i = V_i \times P_i \; \forall i \in \{1, \dots, L\}. \quad (3)$$

The sub-signals, r_i, associated with each principal component are then calculated by averaging along the anti-diagonals of each of the L matrices $\boldsymbol{R}_i$. No information is lost in this process; summing all of the sub-signals will completely reconstruct the original input. The multichannel extension (MSSA) expands one dimension of the trajectory matrix by the number of channels such that spatiotemporal information from all inputs (e.g., measurements made by multiple magnetometers) is leveraged in the decomposition process.

Once the sub-signals have been calculated it is necessary to group them according to their apparent contribution to important geomagnetic phenomena or local magnetic interference generated by the host spacecraft so the interference can be removed. This is done by calculating the statistical correlation between the imperfect interference approximation provided by the magnetic field gradient,

$$\left(\hat{x}_{interference} = x_{inboard} - x_{outboard}\right), \quad (4)$$

and each of the decomposed sub-signals, r_i. A high degree of correlation implies that the sub-signals are morphologically similar to the interference approximation and should be removed. Setting a threshold parameter (α) subsequently determines the confidence of the interference mitigation algorithm and should be tuned accordingly. Further mathematical details and results for the application of this dual-sensor magnetometer denoising technique can be found in (Finley et al., 2023).

2.2 *Machine Learning for Single-Sensor Classification*

Although the field gradient between two magnetometers is useful in classifying decomposed sub-signals as geomagnetic phenomena or local interference, data is not always available from both magnetometers onboard a spacecraft. Often, telemetry limitations force compromises to be made when transmitting magnetic field data to the ground, resulting in limited intervals where two sensors are providing full-cadence measurements. This can obviously limit the applicability of the statistical interference mitigation technique described in Sec. 2.1 due to the unavailability of the interference approximation.

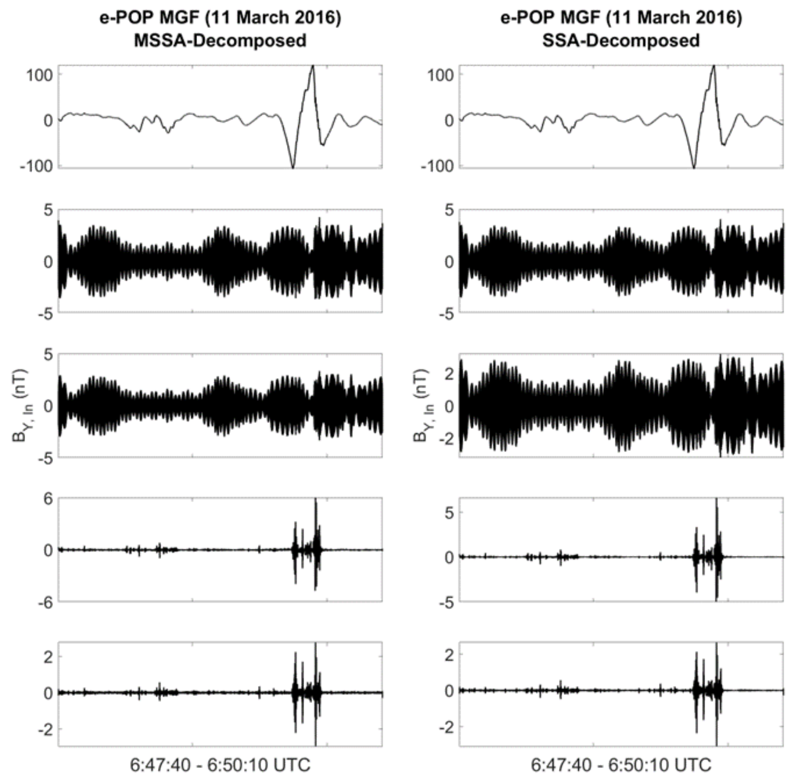

Figure 1: Inboard sensor sub-signals generated by applying MSSA to both sensors (left) and SSA applied only to the inboard sensor (right) on an interval of CASSIOPE/Swarm-Echo magnetic field data.

However, it can be observed that for well-synchronized and calibrated pairs of magnetometers, SSA and MSSA produce extremely similar results. Figure 1 illustrates the first five sub-signals output for the outboard sensor from the dual-sensor MSSA decomposition, as well as the single-sensor SSA decomposition for the outboard sensor, over an interval of CASSIOPE/Swarm-Echo magnetic field data (Wallis et al., 2015; Yau & James, 2015). Note that the same features such as near-DC trend (Row 1), oscillations presumably caused by reaction wheels (Rows 2 and 3), and geomagnetic phenomena (Rows 4 and 5) previously identified as Alfvénic activity (Finley et al., 2023; Miles et al., 2018) can be seen in both methods of decomposition. This implies that the classification of the sub-signals decomposed by both techniques should also be extremely similar, although we cannot rely on the simple field gradient for classification when only one sensor is available.

Recent advances in machine learning (ML) tools have seen neural networks achieve a great deal of success in classifying time-series signals. This manuscript proposes the use of such networks to automatically classify signals decomposed by SSA as either local magnetic interference or residual geophysical signal, enabling interference mitigation even when only a single magnetometer is constantly telemetering data. A high-level block diagram of the proposed technique is shown in Fig. 2a. During intervals where two magnetic field sensors are telemetering data, MSSA is used to decompose the measurements and the magnetic gradient between the sensors is used to classify them, as explained in Sec. 2.1(Finley et al., 2023). These decomposed signals and associated labels are used to train a Convolutional Neural Network (CNN), which is used to perform the same binary classification on SSA-decomposed signals when measurements from only a single magnetometer are available.

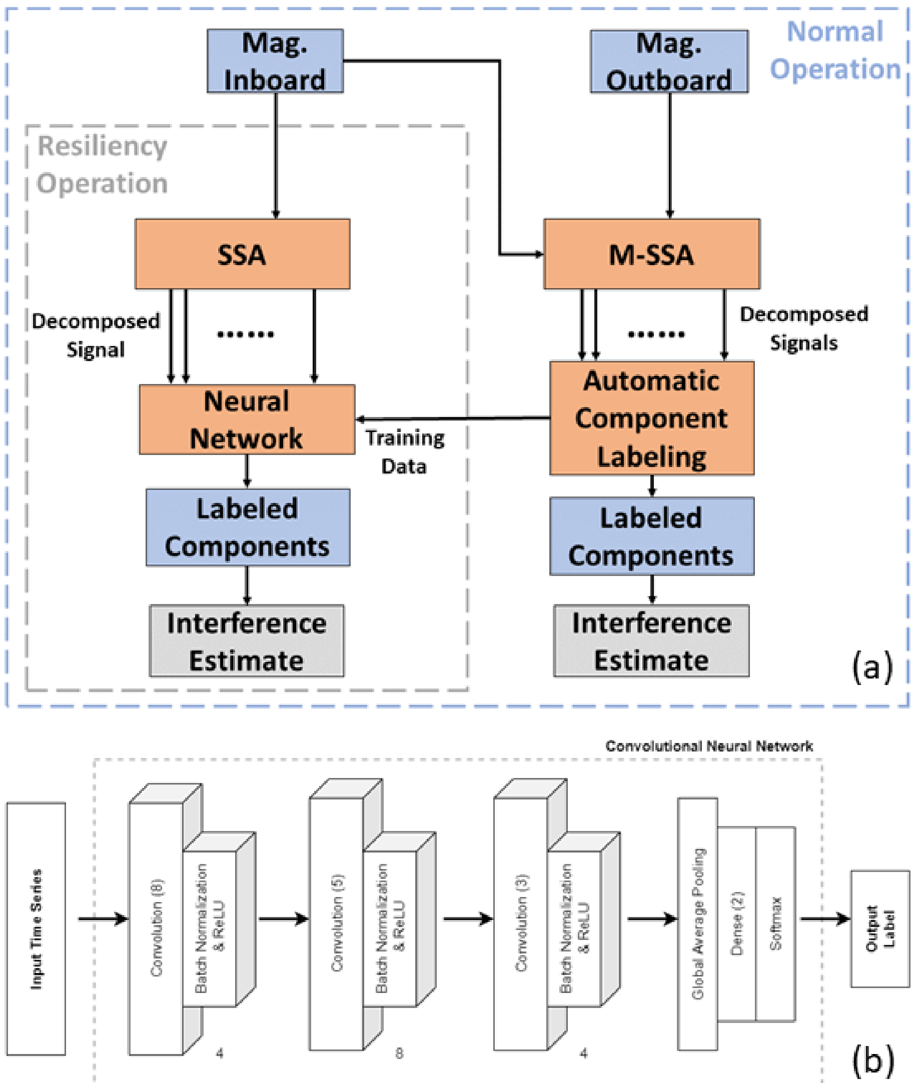

Figure 2: Illustration of the proposed method of interference mitigation applicable to intervals where only a single magnetic field sensor is available. (a) High-level block diagram of proposed method; (b) Specific CNN utilized by the proposed method.

The specific CNN implemented for this manuscript is shown in Fig. 2b, and was adapted from a similar architecture described in (Z. Wang et al., 2017). This network was selected due to the simplicity of its implementation and its performance history on classification of time series data. The basic building block of this network is a convolutional layer followed by batch normalization and the *ReLU* activation function to provide nonlinearity. The filter applied at each convolution decreases in length from eight to five to three for each of the respective blocks. The number of filters applied in each convolutional layer is four for the leftmost and rightmost block, and is eight at the center block. After the convolutions are applied, a global pooling operation is performed, a dense layer is used to adjust the dimensionality, and the *Softmax* activation function provides the probability associated with the binary output labels. This network was implemented in MATLAB 2022b using functionality from the Deep Learning Toolbox. Training parameters and results are discussed in detail in Sec. 4.

3 Data

3.1 *CASSIOPE e-POP/Swarm-Echo MGF*

The first source of data analyzed in this manuscript is from the CASSIOPE/Swarm-Echo magnetic field instrument (MGF). These identical fluxgate magnetometers are deployed on a common boom at distances of approximately 0.9 and 0.6 meters from the host spacecraft. Both sensors measure and telemeter data at a cadence of 160 Sa/sec. The specific intervals chosen for visualization or analysis were selected due to the presence of interesting geophysical events such as the Alfvén waves (Miles et al., 2018) shown in Fig. 1 and ion downflow (Shen et al., 2016, 2018) shown in Sec. 4. Note that a 20-sec mean has been removed from the original measurements captured by the e-POP MGF for ease of visualization.

3.2 *Parker Solar Probe FIELDS MAG*

Another source of data analyzed in this manuscript is from the Parker Solar Probe/FIELDS experiment (Bale et al., 2016). FIELDS consists of two fluxgate magnetometers (MAGs) 1.9 and 2.7 m from the spacecraft, which operate at a maximum sample rate of 292.969 Sa/sec (Bowen, Bale, et al., 2020). The dual sensors provide for failure redundancy, gradiometric estimates of spacecraft noise, and monitoring of variations in DC offsets. The outboard MAG (MAGo) is less impacted by spacecraft noise and accordingly used as the primary science instrument. The inboard MAG (MAGi) is generally run at a lower sample cadence due to telemetry constraints of the mission. Data chosen in this study were chosen due to the identical sample rates of the inboard and outboard measurements. Note that low-frequency interference from other subsystems dominates the field gradient spectrum, and a high-pass filter at 3 Hz is applied to enable isolation of only the reaction wheels, which are a significant source of noise in studying the polarization of plasma waves (Bowen, Mallet, et al., 2020).

4 Results

4.1 *Neural Network Training*

The CNN used to classify decomposed sub-signals on e-POP MGF data was trained using gradiometer data from 1-5 March 2016. The data was split into 40-second intervals (i.e., 6400 samples/interval) and discarded if NaN values were present in either the inboard or outboard measurements (due to data dropouts or other factors). Each of the resulting 476 pairs of measurements were passed through MSSA with a window length of 40, resulting in ~39,000 pairs of sub-signals that were subsequently labeled via correlation against the magnetic field gradient with a threshold of 0.55. This threshold value was intentionally set high to increase the confidence in the labeling scheme, although the resulting labels may still be incorrect when the statistical significance of the sub-signals is ambiguous. Of the original ~76,000 sub-signals, ~2,500 were labeled as interference and ~74,000 were labeled as residual geophysical signal. A random permutation of 2,000 of the sub-signals corresponding to each binary label were selected as inputs to the CNN training.

A similar data processing scheme was utilized for the limited gradiometer data from the Parker Solar Probe MAG. Only three hours of data (06:00:00 – 09:00:00 UTC) from 30 March 2019 (Encounter 2) were processed with a window length of 40 and a threshold value of 0.35, resulting in ~43,000 labeled 40-second intervals (~2,600 labeled as local interference, ~40,500 labeled as residual geophysical signal). A random permutation of 2,500 of the sub-signals corresponding to each label were selected as inputs to the CNN training.

Prior to training the CNN, all input data were normalized between 0 and 1. The total input set was divided randomly into training, validation, and testing sub-sets using a typical 80%, 10%, 10% split. The network was then trained, using the default Adam optimizer (Kingma & Ba, 2017) to minimize the cross-entropy loss function, for ten epochs. Cross-entropy, which calculates the difference between two probability distributions, is a standard choice for classification networks (de Boer et al., 2005). It is important to note that, given the potential for misclassification in the generation of the training set, the performance of the classification network is not necessarily indicative of the performance of the interference mitigation algorithm as a whole. That said, the CNN trained on e-POP MGF data achieved a validation accuracy and loss of 98.0% and 0.086. The CNN trained on PSP MAG data achieved a validation accuracy and loss of 98.86% and 0.046.

4.2 *Numerical Analysis*

To quantitatively assess the performance of the proposed method in mitigating stray magnetic field caused by reaction wheels, it is necessary to perform numerical analysis of the results. This manuscript calculates the linear spectrum associated with the apparent reaction wheel frequencies during the events under observation before and after the application of the proposed method of single-sensor decomposition and ML-enabled sub-signal classification. Results are also calculated for the dual-sensor, gradient-based algorithm to provide a comparison with the technique used to train the classification network.

The values of the linear spectrum associated with the reaction wheel frequencies is calculated using Welch's method of overlapping periodograms (Welch, 1967) and an HFT95 flat-top window with an effective noise bandwidth (ENBW) of 3.8112 Hz (Heinzel et al., 2002). Mathematically, the linear spectrum (LS) can be defined based on the power spectral density (PSD) resulting from Welch's method as

$$LS = \sqrt{PSD \times ENBW}. \tag{5}$$

The results analyzed in this section are from data with near-constant reaction wheel rates for computational simplicity in the absence of a ground truth. Note that, during the intervals selected for analysis, the CASSIOPE reaction wheels were spinning at a uniform rate. As such, only one frequency point must be analyzed to determine the mitigation performance provided by the proposed method. However, the Parker Solar Probe reaction wheels are not at a uniform rate during these intervals, so the linear spectrum value attributed to each reaction wheel frequency (determined using the spacecraft's housekeeping data) is calculated and averaged.

4.3 *Experiments*

The proposed method of automated single-sensor interference mitigation utilizing machine learning classification techniques was applied to four distinct intervals of magnetometer data from two different missions, as shown in Fig. 3. Each row of Fig. 3 corresponds to one interval: Row 1 and 2 illustrate the proposed method applied e-POP MGF data during ion downflow events (Shen et al., 2016, 2018); Row 3 and 4 illustrate the technique applied to intervals of Parker Solar Probe (PSP) MAG data during Encounter 2. The first two columns of Fig. 3 show the outboard measurements before and after the single-sensor correction, as well as after the dual-sensor correction for comparison. Column 1 shows the entire 40-second interval under observation, whereas Column 2 shows a 2-second zoomed view for ease of visualization. Columns 3-5 show the spectra associated with the uncorrected, single-sensor corrected, and dual-sensor corrected measurements, respectively. The red dashed lines overlaid on the spectra correspond to the frequencies of the spacecraft's reaction wheels during these intervals, although this information is not required in the implementation of the proposed interference mitigation technique.

Table 1 provides numerical results for the proposed interference mitigation method using the analysis technique described in Sec. 4.2. The specific frequencies analyzed correspond to the dashed red lines overlaid on the spectra in Fig. 3. For the e-POP MGF events shown, the proposed single-sensor method reduces the amplitude of the frequencies associated with the spacecraft reaction wheels by greater than 87%. For the PSP MAG intervals during Encounter 2, an amplitude reduction of greater than 95% can be seen.

These results are compared to the dual-sensor interference mitigation method, which utilized the same window length (L = 40) as in the single-sensor decomposition, paired with a threshold value of 0.25 for PSP and 0.15 for e-POP. Amplitude reductions of greater than 88% and 78% can be seen for e-POP and PSP, respectively. This slightly lower reduction (specifically for the PSP MAG) can be attributed to the substantial time-frequency overlap seen between the apparent reaction wheel interference and the observed magnetic phenomena during the intervals analyzed.

As the SSA technique and its multivariate extension provide asymptotic separability (Harmouche et al., 2018), larger window lengths enable signal elements with close spectral signatures to be decomposed from one another; however, greater window length also increases the number of sub-signals generated by the decomposition, potentially reducing their statistical significance. As such, an identical window length was used across all experiments for simplicity and consistency. Qualitative analysis of the results displayed in Fig. 3 corroborate this assessment: although both single-sensor and dual-sensor interference mitigation techniques substantially reduce the power at the reaction wheel frequencies, the single-sensor method negates a slightly larger bandwidth surrounding the apparent reaction wheel signature. Although this results in higher numerical accuracy, it is not necessarily indicative of better algorithm performance, and is instead likely an artifact of the limited training set provided to the CNN. More robust models utilizing all available gradiometer data, hyperparameter optimization, and model generalizability across missions are all exciting avenues for future work related to the proposed method of interference mitigation.

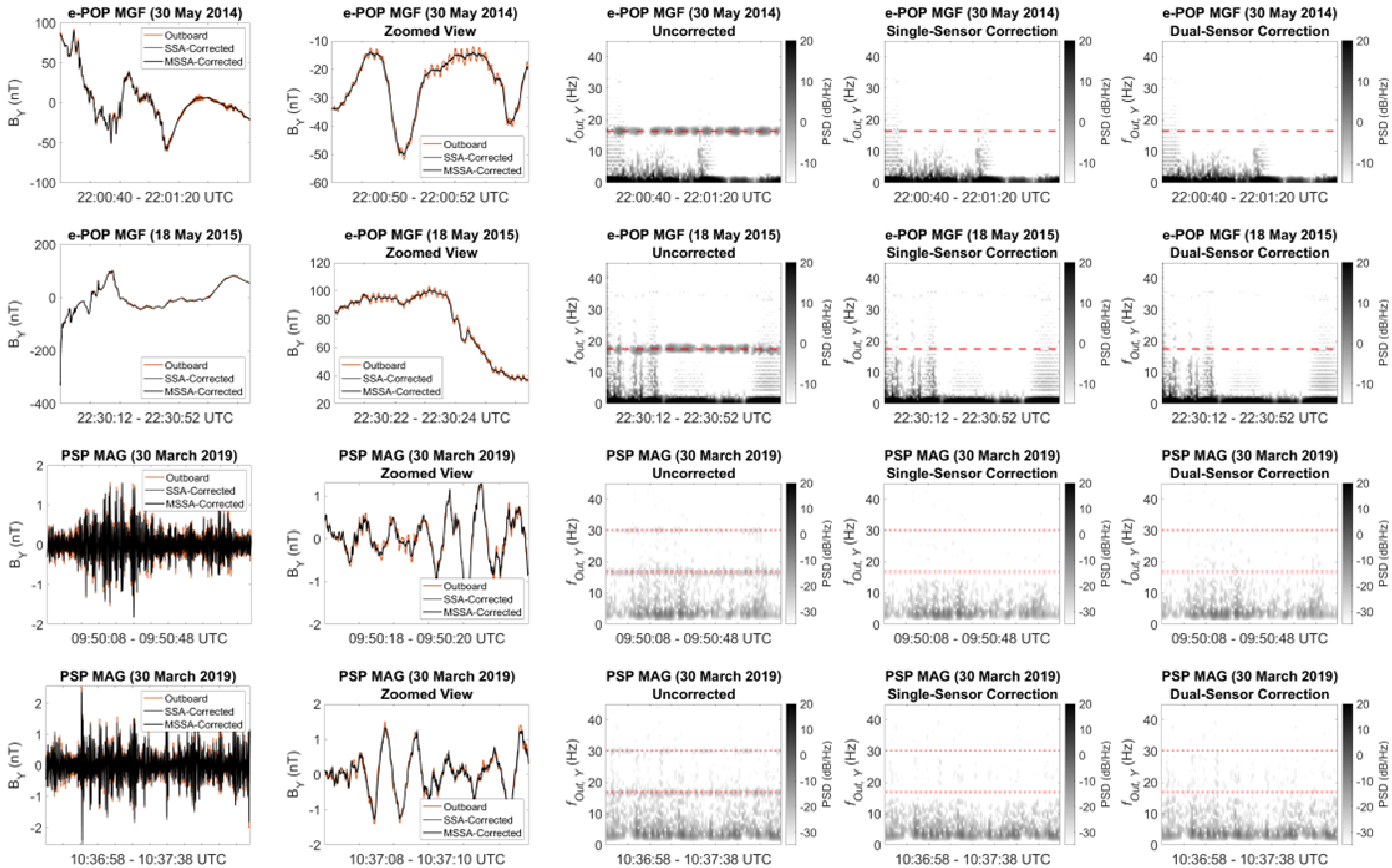

Figure 3: The proposed method of single-sensor interference mitigation compared to dual-sensor mitigation during intervals of e-POP MGF data captured during geomagnetic phenomena (Rows 1-2) and Parker Solar Probe MAG data captured during Encounter 2 (Rows 3-4). (Columns 1-2) Forty-second total interval and two-second zoomed interval time-series data for uncorrected, single-sensor corrected, and dual-sensor corrected outboard measurements; (Column 3) Uncorrected outboard spectrum; (Column 4) Single-sensor corrected outboard spectrum; (Column 5) Dual-sensor corrected outboard spectrum. The dashed red lines indicate the reaction wheel frequencies during each interval.

306 *Table 1: Numerical analysis for the events shown in Fig. 3. (Rows 1-2) Results for interesting geomagnetic intervals captured by the e-POP MGF; (Rows 3-4)*
307 *Results for PSP MAG data captured during Encounter 2.*

	Event	Dominant Wheel Tones	Uncorrected (Linear Spectrum)	SSA-Corrected (Linear Spectrum)	SSA-Corrected (Improvement)	MSSA-Corrected (Linear Spectrum)	MSSA-Corrected (Improvement)
e-POP MGF	**30 May 2014 (22:00:40 UTC)**	16.4 Hz (x4)	1.18 nT	0.15 nT	87.2%	0.04 nT	96.6%
	18 May 2015 (22:30:12 UTC)	17.5 Hz (x4)	0.98 nT	0.07 nT	92.8%	0.11 nT	88.7%
PSP MAG	**30 March 2019 (9:50:08 UTC)**	16.4 Hz, 17.1 Hz, 29.9 Hz, 30.0 Hz	0.042 nT	0.002 nT	95.2%	0.009 nT	78.5%
	30 March 2019 (10:36:58 UTC)	16.6 Hz, 17.1 Hz, 30.0 Hz, 30.1 Hz	0.041 nT	0.002 nT	95.1%	0.007 nT	82.9%

5 Conclusions

This manuscript has presented a novel method for the automatic mitigation of local magnetic interference from sources such as reaction wheels on spacecraft where gradiometer measurements are not always available. Specifically, statistical decomposition and analysis provide a large dataset of labeled sub-signals when gradiometer measurements are available. This dataset is subsequently used to train a neural network to label decomposed signals as local interference or residual physical fields when data from only a single magnetometer is available. This method has been tested, with positive results, against measurements from the CASSIOPE/Swarm-Echo and Parker Solar Probe missions. For example, on a 40-second interval of data during Parker Solar Probe's Encounter 2, a reduction in reaction wheel amplitude of 95.2% can be seen following the application of the proposed method.

Acknowledgments

The CASSIOPE/Swarm-Echo mission is supported by the European Space Agency's Third Party Mission Program. This work was supported in part by the US Air Force Office of Scientific Research (FA9550-21-1-0206). Parker Solar Probe was designed, built, and is now operated by the Johns Hopkins Applied Physics Laboratory as part of NASA's Living With a Star (LWS) program (contract NNN06AA01C).

Open Research

All CASSIOPE/Swarm-Echo MGF data, including the examples used in this manuscript, is publicly available at https://epop-data.phys.ucalgary.ca/. Public access to outboard measurements from Parker Solar Probe MAG is available at https://fields.ssl.berkeley.edu/data/. The Parker Solar Probe MAG inboard data used in this manuscript, as well as the code and data used to generate the figures and analysis, are currently stored at https://iowa-my.sharepoint.com/:f:/g/personal/mgfinley_uiowa_edu/ErDxXKn5NSRGuRP6UqP3050Bm4Vq68Njb3L1dClgfK2ROg. Upon acceptance of this manuscript the code and data will be stored in a University of Iowa Institutional Repository for long-term storage and reuse.

References

Bale, S. D., Goetz, K., Harvey, P. R., Turin, P., Bonnell, J. W., Dudok de Wit, T., Ergun, R. E., MacDowall, R. J., Pulupa, M., Andre, M., Bolton, M., Bougeret, J.-L., Bowen, T. A., Burgess, D., Cattell, C. A., Chandran, B. D. G., Chaston, C. C., Chen, C. H. K., Choi, M. K., … Wygant, J. R. (2016). The FIELDS Instrument Suite for Solar Probe Plus. *Space Science Reviews*, *204*(1), 49–82. https://doi.org/10.1007/s11214-016-0244-5

Bard, C., & Dorelli, J. C. (2021). Neural Network Reconstruction of Plasma Space-Time. *Frontiers in Astronomy and Space Sciences*, *8*. https://www.frontiersin.org/articles/10.3389/fspas.2021.732275

Bowen, T. A., Bale, S. D., Bonnell, J. W., Dudok de Wit, T., Goetz, K., Goodrich, K., Gruesbeck, J., Harvey, P. R., Jannet, G., Koval, A., MacDowall, R. J., Malaspina, D. M., Pulupa, M., Revillet, C., Sheppard, D., & Szabo, A. (2020). A Merged Search-Coil and Fluxgate Magnetometer Data Product for Parker Solar Probe FIELDS. *Journal of Geophysical Research: Space Physics*, *125*(5), e2020JA027813. https://doi.org/10.1029/2020JA027813

Bowen, T. A., Mallet, A., Huang, J., Klein, K. G., Malaspina, D. M., Stevens, M., Bale, S. D., Bonnell, J. W., Case, A. W., Chandran, B. D. G., Chaston, C. C., Chen, C. H. K., Dudok de Wit, T., Goetz, K., Harvey, P. R., Howes, G. G., Kasper, J. C., Korreck, K. E., Larson, D., … The PSP/FIELDS and PSP/SWEAP Teams. (2020). Ion-scale Electromagnetic Waves in the Inner Heliosphere. *The Astrophysical Journal Supplement Series*, *246*(2), 66. https://doi.org/10.3847/1538-4365/ab6c65

Camporeale, E. (2019). The Challenge of Machine Learning in Space Weather: Nowcasting and Forecasting. *Space Weather*, *17*(8), 1166–1207. https://doi.org/10.1029/2018SW002061

Chen, Q., van Dam, T., Sneeuw, N., Collilieux, X., Weigelt, M., & Rebischung, P. (2013). Singular spectrum analysis for modeling seasonal signals from GPS time series. *Journal of Geodynamics*, *72*, 25–35. https://doi.org/10.1016/j.jog.2013.05.005

Clagett, C., Santos, L., Azimi, B., Cudmore, A., Marshall, J., Starin, S., Sheikh, S., Zesta, E., Paschalidis, N., Johnson, M., Kepko, L., Berry, D., Bonalsky, T., Chai, D., Colvin, M., Evans, A., Hesh, S., Jones, S., Peterson, Z., … Rodriquez, M. (2017). Dellingr: NASA

Goddard Space Flight Center's First 6U Spacecraft. *Small Satellite Conference*. https://digitalcommons.usu.edu/smallsat/2017/all2017/83

Clausen, L. B. N., & Nickisch, H. (2018). Automatic Classification of Auroral Images From the Oslo Auroral THEMIS (OATH) Data Set Using Machine Learning. *Journal of Geophysical Research: Space Physics*, *123*(7), 5640–5647. https://doi.org/10.1029/2018JA025274

Constantinescu, O. D., Auster, H.-U., Delva, M., Hillenmaier, O., Magnes, W., & Plaschke, F. (2020). Maximum-variance gradiometer technique for removal of spacecraft-generated disturbances from magnetic field data. *Geoscientific Instrumentation, Methods and Data Systems*, *9*(2), 451–469. https://doi.org/10.5194/gi-9-451-2020

de Boer, P.-T., Kroese, D. P., Mannor, S., & Rubinstein, R. Y. (2005). A Tutorial on the Cross-Entropy Method. *Annals of Operations Research*, *134*(1), 19–67. https://doi.org/10.1007/s10479-005-5724-z

Finley, M. G., Broadfoot, R. M., Shekhar, S., & Miles, D. M. (2023). Identification and Removal of Reaction Wheel Interference From In-Situ Magnetic Field Data Using Multichannel Singular Spectrum Analysis. *Journal of Geophysical Research: Space Physics*, *128*(2), e2022JA031020. https://doi.org/10.1029/2022JA031020

Golyandina, N., Nekrutkin, V., & Zhigljavsky, A. A. (2001). *Analysis of Time Series Structure: SSA and Related Techniques*. CRC Press.

Groth, A., & Ghil, M. (2015). Monte Carlo Singular Spectrum Analysis (SSA) Revisited: Detecting Oscillator Clusters in Multivariate Datasets. *Journal of Climate*, *28*(19), 7873–7893. https://doi.org/10.1175/JCLI-D-15-0100.1

Harmouche, J., Fourer, D., Auger, F., Borgnat, P., & Flandrin, P. (2018). The Sliding Singular Spectrum Analysis: A Data-Driven Nonstationary Signal Decomposition Tool. *IEEE Transactions on Signal Processing*, *66*(1), 251–263. https://doi.org/10.1109/TSP.2017.2752720

Hassani, H., Soofi, A. S., & Zhigljavsky, A. A. (2010). Predicting daily exchange rate with singular spectrum analysis. *Nonlinear Analysis: Real World Applications*, *11*(3), 2023–2034. https://doi.org/10.1016/j.nonrwa.2009.05.008

Hassani, H., & Thomakos, D. (2010). A review on singular spectrum analysis for economic and financial time series. *Statistics and Its Interface*, *3*(3), 377–397. https://doi.org/10.4310/SII.2010.v3.n3.a11

Heinzel, G., Rudiger, A., & Schilling, R. (2002). *Spectrum and spectral density estimation by the Discrete Fourier transform (DFT), including a comprehensive list of window functions and some new flat-top windows.*

Hoffmann, A. P., & Moldwin, M. B. (2022). Separation of Spacecraft Noise From Geomagnetic Field Observations Through Density-Based Cluster Analysis and Compressive Sensing. *Journal of Geophysical Research: Space Physics*, *127*(9), e2022JA030757. https://doi.org/10.1029/2022JA030757

Imajo, S., Nosé, M., Aida, M., Matsumoto, H., Higashio, N., Tokunaga, T., & Matsuoka, A. (2021). Signal and Noise Separation From Satellite Magnetic Field Data Through Independent Component Analysis: Prospect of Magnetic Measurements Without Boom and Noise Source Information. *Journal of Geophysical Research: Space Physics*, *126*(5), e2020JA028790. https://doi.org/10.1029/2020JA028790

Kingma, D. P., & Ba, J. (2017). *Adam: A Method for Stochastic Optimization* (arXiv:1412.6980). arXiv. https://doi.org/10.48550/arXiv.1412.6980

Kletzing, C. A., Kurth, W. S., Acuna, M., MacDowall, R. J., Torbert, R. B., Averkamp, T., Bodet, D., Bounds, S. R., Chutter, M., Connerney, J., Crawford, D., Dolan, J. S., Dvorsky, R., Hospodarsky, G. B., Howard, J., Jordanova, V., Johnson, R. A., Kirchner, D. L., Mokrzycki, B., … Tyler, J. (2013). The Electric and Magnetic Field Instrument Suite and Integrated Science (EMFISIS) on RBSP. *Space Science Reviews*, *179*(1), 127–181. https://doi.org/10.1007/s11214-013-9993-6

Miles, D. M., Mann, I. R., Pakhotin, I. P., Burchill, J. K., Howarth, A. D., Knudsen, D. J., Lysak, R. L., Wallis, D. D., Cogger, L. L., & Yau, A. W. (2018). Alfvénic Dynamics and Fine Structuring of Discrete Auroral Arcs: Swarm and e-POP Observations. *Geophysical Research Letters*, *45*(2), 545–555. https://doi.org/10.1002/2017GL076051

Miller, D. C. (1979, April 1). *The Voyager magnetometer boom*. https://ntrs.nasa.gov/citations/19790013187

Ness, N. F., Behannon, K. W., Lepping, R. P., & Schatten, K. H. (1971). Use of two magnetometers for magnetic field measurements on a spacecraft. *Journal of Geophysical Research (1896-1977)*, *76*(16), 3564–3573. https://doi.org/10.1029/JA076i016p03564

Sheinker, A., & Moldwin, M. B. (2016). Adaptive interference cancelation using a pair of magnetometers. *IEEE Transactions on Aerospace and Electronic Systems*, *52*(1), 307–318. https://doi.org/10.1109/TAES.2015.150192

Shen, Y., Knudsen, D. J., Burchill, J. K., Howarth, A. D., Yau, A. W., Miles, D. M., James, H. G., Perry, G. W., & Cogger, L. (2018). Low-Altitude Ion Heating, Downflowing Ions, and BBELF Waves in the Return Current Region. *Journal of Geophysical Research: Space Physics*, *123*(4), 3087–3110. https://doi.org/10.1002/2017JA024955

Shen, Y., Knudsen, D. J., Burchill, J. K., Howarth, A., Yau, A., Redmon, R. J., Miles, D. M., Varney, R. H., & Nicolls, M. J. (2016). Strong ambipolar-driven ion upflow within the cleft ion fountain during low geomagnetic activity. *Journal of Geophysical Research: Space Physics*, *121*(7), 6950–6969. https://doi.org/10.1002/2016JA022532

Smola, J. F., Radford, W. E., & Reitz, M. H. (1980, May 1). *The Magsat magnetometer boom*. https://ntrs.nasa.gov/citations/19800015026

Styp-Rekowski, K., Michaelis, I., Stolle, C., Baerenzung, J., Korte, M., & Kao, O. (2022). Machine learning-based calibration of the GOCE satellite platform magnetometers. *Earth, Planets and Space*, *74*(1), 138. https://doi.org/10.1186/s40623-022-01695-2

Tian, C., Xu, Y., Fei, L., & Yan, K. (2019). Deep Learning for Image Denoising: A Survey. In J.-S. Pan, J. C.-W. Lin, B. Sui, & S.-P. Tseng (Eds.), *Genetic and Evolutionary Computing* (pp. 563–572). Springer. https://doi.org/10.1007/978-981-13-5841-8_59

Vautard, R., & Ghil, M. (1989). Singular spectrum analysis in nonlinear dynamics, with applications to paleoclimatic time series. *Physica D: Nonlinear Phenomena*, *35*(3), 395–424. https://doi.org/10.1016/0167-2789(89)90077-8

Wallis, D. D., Miles, D. M., Narod, B. B., Bennest, J. R., Murphy, K. R., Mann, I. R., & Yau, A. W. (2015). The CASSIOPE/e-POP Magnetic Field Instrument (MGF). *Space Science Reviews*, *189*(1), 27–39. https://doi.org/10.1007/s11214-014-0105-z

Wang, E., & Nealon, J. (2019). Applying machine learning to 3D seismic image denoising and enhancement. *Interpretation*, *7*(3), SE131–SE139. https://doi.org/10.1190/INT-2018-0224.1

Wang, Z., Yan, W., & Oates, T. (2017). Time series classification from scratch with deep neural networks: A strong baseline. *2017 International Joint Conference on Neural Networks (IJCNN)*, 1578–1585. https://doi.org/10.1109/IJCNN.2017.7966039

Welch, P. (1967). The use of fast Fourier transform for the estimation of power spectra: A method based on time averaging over short, modified periodograms. *IEEE Transactions on Audio and Electroacoustics*, *15*(2), 70–73. https://doi.org/10.1109/TAU.1967.1161901

Yau, A. W., & James, H. G. (2015). CASSIOPE Enhanced Polar Outflow Probe (e-POP) Mission Overview. *Space Science Reviews*, *189*(1), 3–14. https://doi.org/10.1007/s11214-015-0135-1